

Investigation of Wideband Two Elements Dual Segment Half-Cylindrical Dielectric Resonator Antenna (DS h-CDRA) with RCS Analysis

Pinku Ranjan^{1, *}, Ravi K. Gangwar², Abhishek P. Singh¹, and Ayush Varshney¹

Abstract—In this paper dual segment half Cylindrical Dielectric Resonator Antennas (DS h-CDRA), deploying homogenous elements, are designed and analyzed for wide-band applications. At first a single element is analyzed followed by two element DS h-CDRA. Further, Radar Cross Section (RCS) analysis is performed for different angles and frequencies. The proposed antennas are excited from the center of the ground plane using a coaxial probe feed, which results in $\mathbf{TM}_{01\delta}$ as a mode of excitation in cylindrical DRA. The input impedance and radiation characteristics are determined and compared with measured results, which shows good agreement. The proposed DS h-CDRA provides measured wide bandwidth ($\approx 98\%$) from 5.0 GHz to 11.5 GHz with gain of 4.85 dBi, and it is found constant throughout the operational band (with omnidirectional radiation pattern). The designed antennas performance has also been compared with two element h-CDRA and found even better for the same volume and effective radiation area. The RCS analysis has been performed for monostatic and bistatic mode at different frequencies and angles. The proposed antenna has been found suitable for 5.0 GHz WLAN and WiMAX wireless application.

1. INTRODUCTION

Dielectric resonators (DRs) can act as an efficient radiator and used as an antenna, once it is left in open environment. Material having high dielectric constant (ϵ_r) and low loss tangent ($\tan \delta \approx 10^{-4}$) has been used for fabrication of DRAs. In the beginning, Long et al. [2] investigated a cylindrical dielectric resonator for providing efficient radiation with some enticing options and characteristics namely zero conductor losses, high radiation efficiency, small size, light weight and ease of excitation that make it appropriate for wireless applications [1–3]. Mode of excitation and shape/size of the DRA is the most important thing for radiation characteristics. Some of the fundamental modes have been investigated for cylindrical dielectric resonator antenna CDRA, namely \mathbf{TE}_{01} , $\mathbf{TM}_{01\delta}$, $\mathbf{HE}_{11\delta}$, $\mathbf{EH}_{11\delta}$, and $\mathbf{TE}_{011+\delta}$ [3]. DRA does not support surface wave and ohmic loss, which leads to its high radiation efficiency [2–4].

Recently, bandwidth enhancement is a major concern for antenna designers. Several approaches have been investigated by researchers for bandwidth enhancement, such as changing the aspect ratio of DRA [5], using multi-element concept [6], using stacking and multi-segments [7–10], sectoring/splitting of the basic structure [11–14] and an air gap introduction below the DRA [15–17]. An experiment was performed by Petosa et al. with multi-segment approach for rectangular DRA, to get wideband in which low dielectric material was inserted below the DRA [7]. For the improvement in bandwidth, stacking of a annular ring DRA has been introduced by Luk and Shum with coaxial probe feed [8]. The triangular DRA with segmentation approach has been investigated for bandwidth improvement

Received 31 May 2018, Accepted 12 July 2018, Scheduled 26 July 2018

* Corresponding author: Pinku Ranjan (pinkuranjan@ece.ism.ac.in).

¹ Department of ECE, SRM Institute of Science and Technology, Kattankulathur, Chennai, India. ² Department of Electronics Engineering, Indian Institute of Technology (Indian School of Mines), Dhanbad, India.

and found to have 35% bandwidth [10]. The splitting of the basic cylindrical shape has been proposed by Mongia et al. [11, 12] with bandwidth improvement for monopole type radiation pattern to enhance the bandwidth of the DRA. When a compact cylindrical sector DRA is compared with conventional CDRA, it is found that there is a decrement in volume by 75% [14]. The air gap has been introduced below the DRA to enhance the bandwidth [15–17].

The monopole type of radiation pattern has been described by some researchers for various DRA shapes [18–22]. In the beginning, monopole type radiation pattern was reported by Mongia et al. [18] using dielectric resonator. For $TM_{01\delta}$ mode excitation, a circular pattern dielectric ring resonator was powered by a central coaxial probe feed. The monopole like radiation pattern has also been demonstrated by Guha and Antar [6] for four elements CDRA which shows nearly 29% impedance bandwidth. Half split hemispherical DRAs were investigated as broadband variants of low profile monopole type DRAs with 35% bandwidth enhancement in [9]. Multi-element concept was investigated for various forms to improve the bandwidth such as four elements rectangular and triangular DRAs, which provides 35% bandwidth with monopole like radiation pattern [21, 22].

The radar cross section (RCS) analysis of antenna has been investigated as an object involving a stealth technology, which should be as low as possible. The antenna/radar signature is proportional to the reflections from antenna surface; RCS analysis significantly increases with the use of antennas in military applications. Therefore, RCS analysis and its reduction have attracted great interest from researchers over the last few years [24–27]. The RCS analysis will explore the orientation of antenna while deploying based on application. In the monostatic case, the proposed antenna orientation has to be kept at 0° angles, while bistatic case different-different angle orientation has to be considered.

This paper presents the concept of sectoring of the basic cylindrical shape along with multi-element and multi-segment approach for wide bandwidth and monopole type radiation pattern. The design and development of the projected MEMS h-CDRA are investigated through the Ansoft HFSS simulation software system. The prototype of the proposed DRA has been fabricated. The simulated antenna performance has been verified through measurement. The proposed antenna shows 98% bandwidth ($|S_{11}| \leq -10$ dB) with uniform monopole-like radiation pattern for the complete operating frequency band. The input characteristics of the two elements DS h-CDRA have been compared with the DS h-CDRA. The RCS analysis has been performed for proposed antenna. The monostatic and bistatic RCS analyses have been carried out for different frequencies and different angles.

2. ANTENNA DESIGN AND ANALYSIS

The half split cylindrical sector dielectric resonator antenna (h-CDRA) has been built through cutting vertically in two uniform equal half of a solid cylinder. The dual-segmentation (DS) approach has been imposed in the h-CDRA to make a dual-segment half split cylindrical dielectric resonator antenna (DS h-CDRA), which is shown in Fig. 1. The h-CDRA has been constructed with a sector of an arbitrary angle β . Its sectored face has been left open so that approximately magnetic wall boundary conditions can be imposed on it [3].

By assuming a magnetic wall approximation for complete surface of h-CDRA, the field inside the cylindrical sector DRA in terms of TM_{mnp} modes is [1, 3]

$$E_z^{mnp} = [AJ_m(k_r r) + BY_m(k_r r)] [C \sin(v\theta) + D \cos(v\theta)] \cos(k_z z) \quad (1)$$

Here A , B , C and D are arbitrary constants which depend on position and feed of the DRA. J_m , Y_m denote the first and second kind m th-order Bessel functions, respectively, where m is the positive real number which depends upon boundary conditions, and n , p are positive integers. Here for simplicity purpose, coaxial probe feed is chosen.

The resonant frequency of TM_{mnp} mode:

$$k_r^2 + k_z^2 = k^2 = \epsilon_{r,eff} \left(\frac{2\pi f}{c} \right)^2 \quad (2)$$

where $k_r = \frac{X'_{mn}}{a}$, $k_z = \frac{(2p+1)\pi}{2h_{eff}}$ are wavenumbers.

X'_{mn} is the root satisfying $J_m'(X'_{mn}) = 0$.

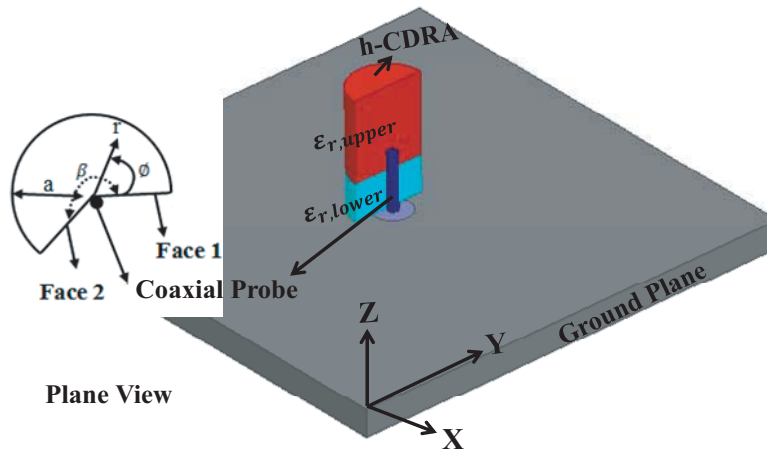


Figure 1. Geometry of segmented cylindrical sector h-CDRA.

So the final equation for the resonant frequency of h-CDRA calculated for TM_{mnp} mode is [1, 3]

$$f_{mnp} = \frac{c}{2\pi a \sqrt{\mu_r \epsilon_{r,eff}}} \sqrt{X_{mn}^2 + \left[\frac{\pi a}{2h_{eff}} (2p + 1) \right]^2} \quad (3)$$

Here for h-CDRA $\beta = 180^\circ$, so it makes DS h-CDRA through stacking of the two different dielectric materials. Here $\epsilon_{r,eff}$ and h_{eff} are defined as

$$\epsilon_{r,eff} = \frac{h_{eff}}{h_{lower}/\epsilon_{r,lower} + h_{upper}/\epsilon_{r,upper}} \quad \text{and} \quad h_{eff} = h_{lower} + h_{upper} \quad (4)$$

Using Equation (4), approximately effective dielectric constant and height have been calculated. From Equation (3), it can be observed that the resonant frequency is inversely proportional to the effective dielectric constant of the material. Further, the Q-factor of the proposed antenna will decrease with decrease of dielectric constant and tangent loss ($\tan \delta = 0.002$ for Alumina and $\tan \delta = 0.001$ for Teflon), which will result in bandwidth enhancement.

The sectored face has been left open so that it forms approximate magnetic walls. The magnetic walls on faces 1 and 2 have the boundary conditions

$$\begin{aligned} \frac{\partial E_z}{\partial \phi} &= 0 \text{ at } \phi = 0 \text{ and } \phi = \beta, \\ n &= \frac{v\pi}{\beta} \text{ where } 0 < \beta \leq 2\pi \end{aligned} \quad (5)$$

Here face 1 and face 2 are combined and make a single face on which above boundary conditions can be imposed.

Here v is a nonzero positive integer to satisfy the boundary conditions at open face. The solution for open face requires the condition $C = 0$. The resonant frequency depends on radius and height of the DS h-CDRA for a particular mode. The resonant frequency for $TM_{01\delta}$ mode of the DS h-CDRA is calculated using Equation (3) for $0 < \delta < 1$. The calculated value of resonant frequency exists between 6.5 GHz and 9.25 GHz depending upon ‘ δ ’ value.

The two elements DS h-CDRA has been designed using two DS h-CDRAs, which are kept in such a way that the coaxial probe touches the center of DS h-CDRAs to excite the proposed antenna. The performance of the proposed antenna with dual-segment approach is tabulated in Table 1 and Table 2. From Table 1 and Table 2, it can be observed that the bandwidth enhancement can be achieved through the low dielectric material kept below the high dielectric material.

From the above analysis, DS h-CDRA has been made up of combining two segments (lower segment and upper segment). The DS h-CDRA has been designed with Ansoft HFSS simulation software and

Table 1. Variation of segment thickness and dielectric constant of two elements DS h-CDRA for lower segment [$h_{upper} = h_{eff} - h_{lower}$, $\epsilon_{r,upper} = 9.8$, effective height (h_{eff}) = 13 mm].

h_{lower} (mm)	h_{upper} (mm)	$\epsilon_{r,lower} = 2.1$		$\epsilon_{r,lower} = 4.4$		$\epsilon_{r,lower} = 6.0$	
		% B.W	f_r (GHz)	% B.W	f_r (GHz)	% B.W	f_r (GHz)
1	12	54.32	5.8	41.32	5.3	36.23	5.2
2	11	67.66	6.1	52.67	5.7	45.86	5.4
3	10	81.30	6.45	58.00	6.1	54.40	5.5
4	9	98.46	6.5	63.49	6.3	57.62	5.9
5	8	91.54	6.7	68.45	6.4	61.50	6.1

Table 2. Antenna performance with segment arrangement of two elements DS h-CDRA, effective height (h_{eff}) = 13 mm.

Lower Segment		Upper Segment		Operating Bandwidth (GHz)	Resonant Frequency (f_r) GHz	% Bandwidth	Gain (dBi)
ϵ_{r1}	h_1 (mm)	ϵ_{r2}	h_2 (mm)				
2.1	4.0	9.8	9.0	5.0–11.4	6.5	98.46	4.85
9.8	4.0	2.1	9.0	4.5–6.5	5.4	37.03	4.70
9.8	9.0	2.1	4.0	5.1–8.8	7.4	50.00	4.15
2.1	9.0	9.8	4.0	6.1–9.4	7.6	43.42	4.60
4.4	4.0	9.8	9.0	5.2–9.2	6.3	63.49	4.25
6.0	4.0	9.8	9.0	4.7–8.1	5.9	57.62	4.15

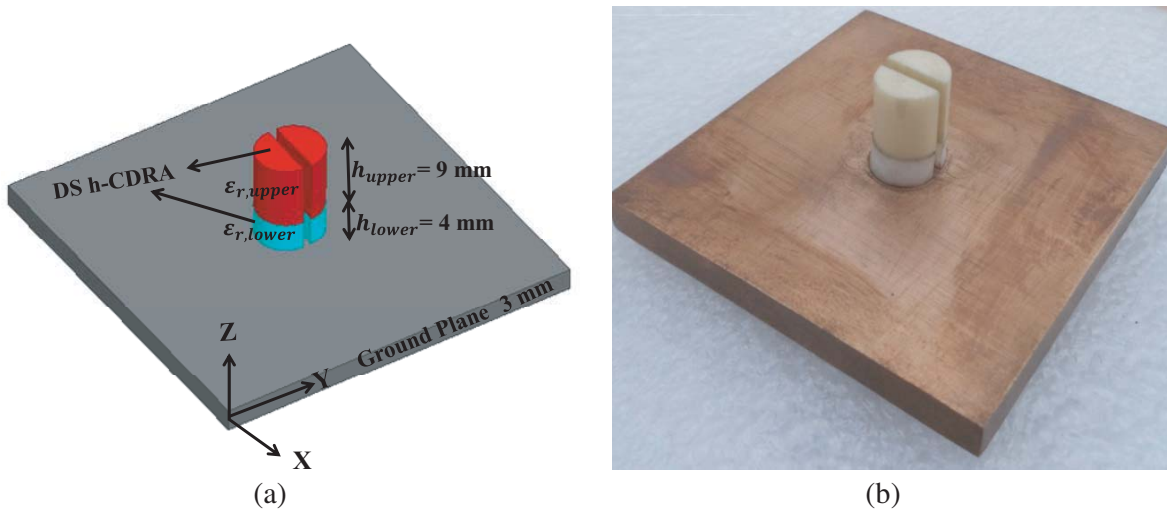


Figure 2. (a) Geometry and (b) fabricated prototype of proposed two elements DS h-CDRA.

fabricated, as shown in Fig. 2. The dielectric constant has been chosen as the upper layer ($\epsilon_{r,upper}$) 9.8 (Alumina ceramic) and the lower layer ($\epsilon_{r,lower}$) 2.1 (Teflon) with very low tangent loss. The height of the DS h-CDRA has been optimized for minimum reflection coefficient and maximum bandwidth. The heights of upper and lower layers are 9 mm and 4 mm, respectively. The radius of the CDRA has been kept constant 4 mm for both segments. The dimension of ground plane has been obtained

50 mm × 50 mm × 3 mm through simulation. The dimension of the DRA is very low compared to the dimension of the ground plane, so that it can be assumed that the ground plane behaves as infinite ground plane for the proposed antenna. An adhesive material (fewquick) has been used for fixing the DRA on the ground plane in the fabrication process. In the fabrication process, the SMA connector has been fitted at the center of the ground plane as shown in Fig. 2(b). The probe height has been optimized through extensive simulations for minimum reflection coefficient and obtained as 9.2 mm from the bottom of the ground plane.

3. RESULTS AND DISCUSSION

The reflection coefficient versus frequency curve of the proposed h-CDRA is shown in Fig. 3. The measurement of input characteristics of the proposed DS h-CDRAs has been performed by using Rohde & Schwarz Vector Network Analyzer (Model No. ZVM, 10 MHz–20 GHz), and the extracted data of input characteristics have been analyzed. The simulated results have been compared with measured ones. The slight mismatch is observed in the proposed antenna performance due to the fabrication error. From Fig. 3, the resonant frequency and operating frequency range vary, and therefore, the percentage bandwidth of the DS h-CDRAs has been extracted and shown in Table 3. Two elements DS h-CDRA provides wide bandwidth (~ 98.48%) and covers complete 5.0 GHz WLAN and WiMAX band which is observed from Fig. 3 and Table 3. The proposed two elements DS h-CDRA has wide bandwidth, which might be because of increment in radiation volume and area, lower resonant frequency in contrast to DS h-CDRA [14]. The proposed antennas have been designed in such a way that without changing the dimensions and volume of cylindrical DRA, it is still able to enhance the bandwidth (achieving 98%) as well as gain (4.85 dBi). Compared to other shapes (triangle, rectangle, hemisphere, and cylinder), half-split cylindrical DRA has reduced volume and area. The proposed antenna dimension is very low compared to above mentioned shapes, but performance wise it is better than other DRAs as shown in Table 4. From Table 4, it can be observed that the proposed antenna has least radiated area even showing better performance than other previous published designs.

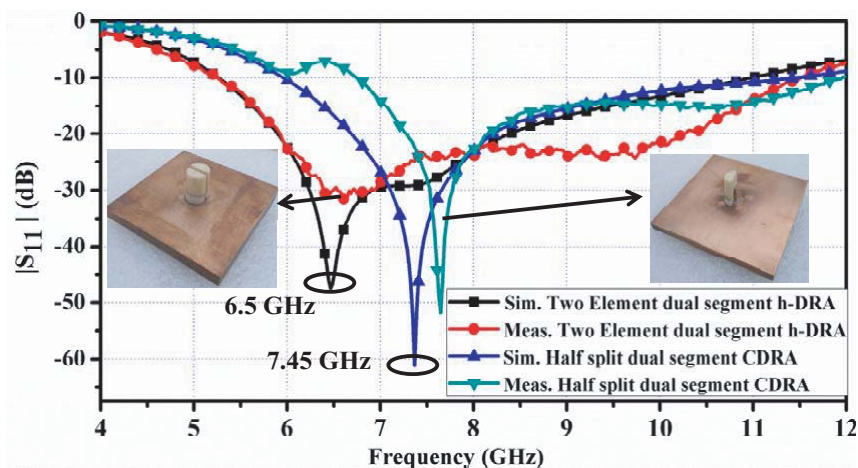


Figure 3. $|S_{11}|$ versus frequency curves of proposed two elements DS h-CDRA compared with DS h-CDRA.

Fig. 4 illustrates the information about the input impedance and frequency characteristics of the planned antenna which has been analyzed by using an Ansoft HFSS. By observing the graph, at the resonant frequency (6.6 GHz) the values of measured and simulated input resistances are 52.54 Ω and 50.5 Ω , respectively. The calculated and simulated input resistances provide a close agreement and also show a satisfactory resistance match with 50 Ω coaxial probe feed.

The near-field distributions of the designed antenna have been observed at resonant frequency 6.6 GHz using Ansoft HFSS simulation software. The dispersions of E-field and H-field appear in

Table 3. The performance of two elements DS h-CDRA and DS h-CDRA.

Parameter	Geometry	Dual segment h-CDRA (DS h-CDRA)		Proposed DS h-CDRA	
		Simulated	Measured	Simulated	Measured
Operating frequency range ($ S_{11} \leq -10$ dB)		5.8–11.8 GHz	6.0–12.0 GHz	5.0–11.4 GHz	5–11.5 GHz
Resonant frequency		7.45 GHz	7.6 GHz	6.5 GHz	6.6 GHz
% Bandwidth		80.53%	78.94%	98.46%	98.48%

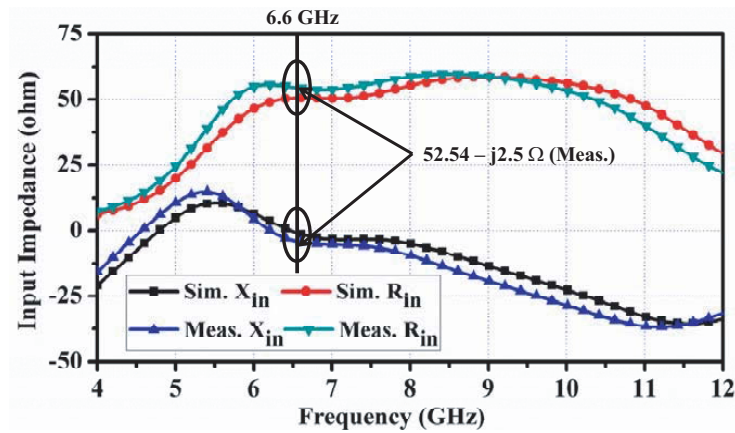


Figure 4. Variation of input impedance vs. frequency of proposed two elements DS h-CDRA.

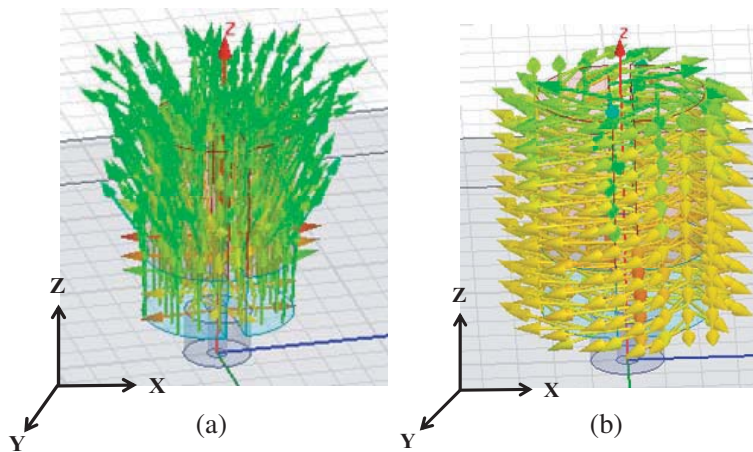


Figure 5. (a) E-field and (b) H-field distribution in proposed two elements DS h-CDRA.

Fig. 5(a) and Fig. 5(b), respectively. It can be seen from Fig. 5 that $TM_{01\delta}$ dominates the mode energized in the proposed design. It is obvious from Fig. 5(a) that the electric field segments confront their counter vectors in XY plane and in this manner causes no radiation along the broadside course. The ensuing electrical field’s square measure polarized on coordinate z -axis and therefore causes a vertically polarized radiation encompassing the diverging structure sort of a quarter wave particle.

By using Ansoft HFSS simulation software, the pattern for the far field is examined. Radiation pattern of the projected antenna has been measured inside an anechoic chamber. The simulated and measured radiation patterns of the proposed two components DS h-CDRA have been analysed for both E -plane (XZ and YZ plane) and H -plane (XY plane) at the the resonant frequency (6.6 GHz) which

Table 4. Comparison of the proposed antenna with previous published structures.

S. No.	Shape of DRA	DRA Radiation Area (mm ²)	Operating Bandwidth	Percentage Bandwidth ($ S_{11} \leq -10$ dB)	Resonant Frequency (f_r)	References
1.	Four element Cylinder	1570.00	3.0–4.0 GHz	29%	3.4 GHz	[6]
2.	Half Hemisphere	2513.27	2.8–4.2 GHz	35%	3.7 GHz	[9]
3.	Four element Triangular with dual segment	924.00	5.5–7.8 GHz	33%	6.9 GHz	[10]
4.	Half split Cylinder	1687.00	6.6–7.6 GHz	8%	6.87 GHz	[11]
5.	Half split Cylinder	2354.00	7.08–7.83 GHz	10%	7.43 GHz	[12]
6.	Half split Cylinder	1854.00	1.7–2.3 GHz	35%	2.1 GHz	[13]
7.	Cylindrical sector	1085.51	1.68–2.30 GHz	10%	1.8 GHz	[14]
8.	Four element Rectangular	1904.00	5.0–7.0 GHz	35%	5.7 GHz	[21]
9.	Four element Triangular	924.00	4.7–6.8 GHz	37%	5.45 GHz	[22]
10.	Half split Cylinder	239.00	5.1–8.3 GHz	51%	6.25 GHz	[28]
11.	Proposed three elements dual segment t-CDRA	213.62	5.0–11.5 GHz	98%	6.6 GHz	Present Paper

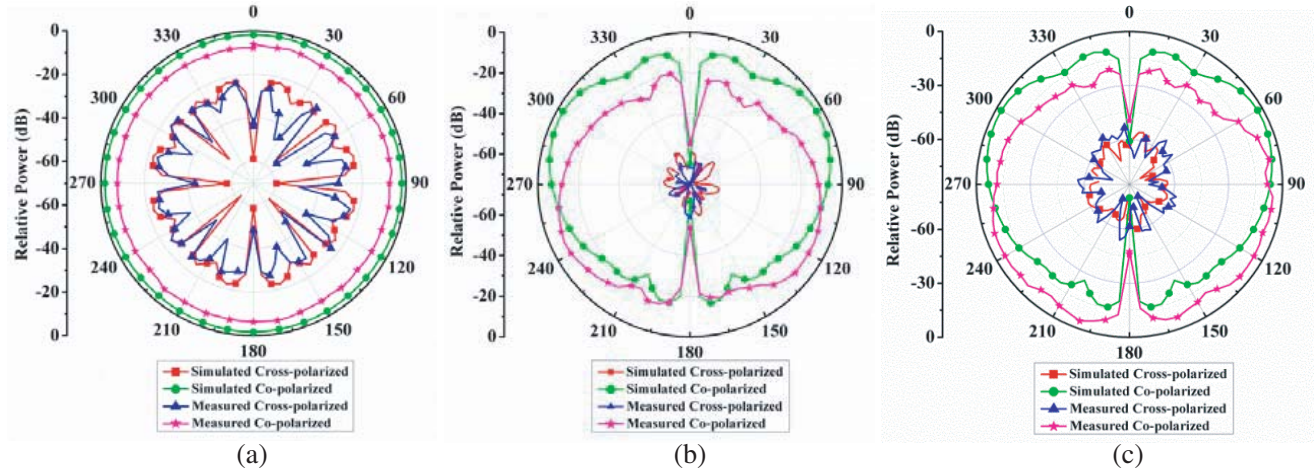


Figure 6. Radiation pattern of proposed two elements DS h-CDRA, (a) in XY plane, (b) in YZ plane, (c) in ZX plane at resonant frequency 6.6 GHz.

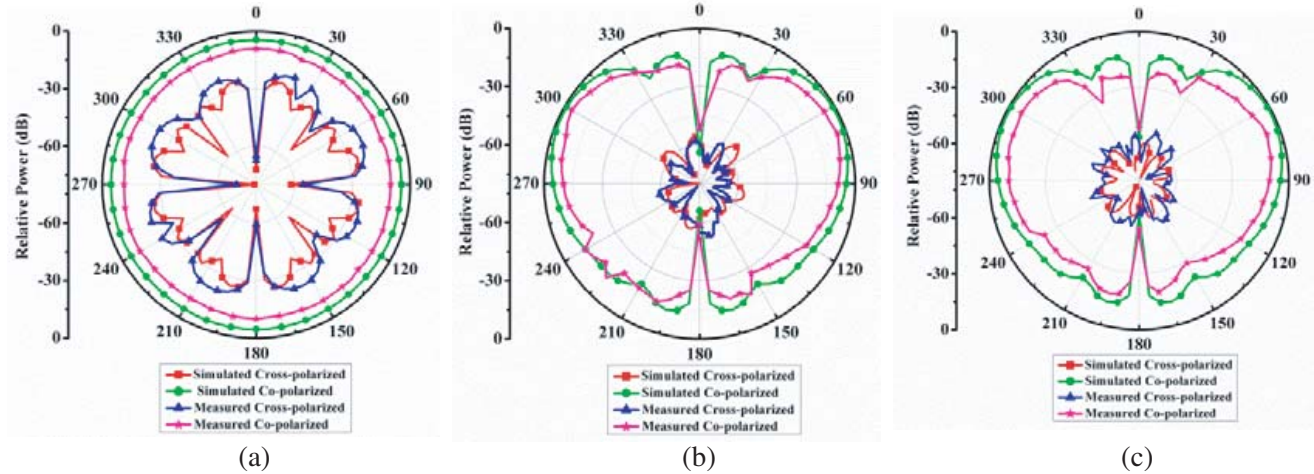


Figure 7. Radiation pattern of proposed two elements DS h-CDRA, (a) in ZX -plane, (b) in YZ -plane, (c) in XY -plane at frequency 5.5 GHz.

appears in Fig. 6. The simulated and measured radiation patterns have likewise been seen at two more frequencies 5.5 GHz and 8 GHz to confirm the radiation pattern for the whole operating working band in every one of the three planes, which appear in Fig. 7 and Fig. 8 individually. Figs. 6(a), 7(a) and 8(a) demonstrate H -plane ($\theta = 90^\circ$ for XY -plane) radiation pattern at various frequencies for the proposed antenna. Similarly Figs. 6(b), 7(b) and 8(b) show E -plane at $\phi = 0^\circ$ (for ZX -plane), and Figs. 6(c), 7(c) and 8(c) demonstrate E -plane at $\phi = 90^\circ$ (for YZ -plane) radiation pattern at various frequencies. The cross polarization level has 20 dB down w.r.t to copolarization level in E -plane and also H -plane. The proposed antenna has omnidirectional radiation pattern in H -plane which is observed from Figs. 6, 7 and 8. The proposed antenna has a monopole like radiation pattern in E -plane with null at broadside direction due to $TM_{01\delta}$ mode. No radiation along broadside of the antenna has confirmed that the counteracting E -field distributions within the elements of the DRA [17].

Figure 9 shows the gain versus frequency curves of the proposed antenna. Three antenna method [23] has been used for gain measurement at a tilted direction of $\theta = 60^\circ$. The gain has a maximum value of 4.85 dBi which can be extracted from Fig. 9). Measured and simulated gains have a close agreement with each other. The gains of the proposed two elements DS h-CDRA have

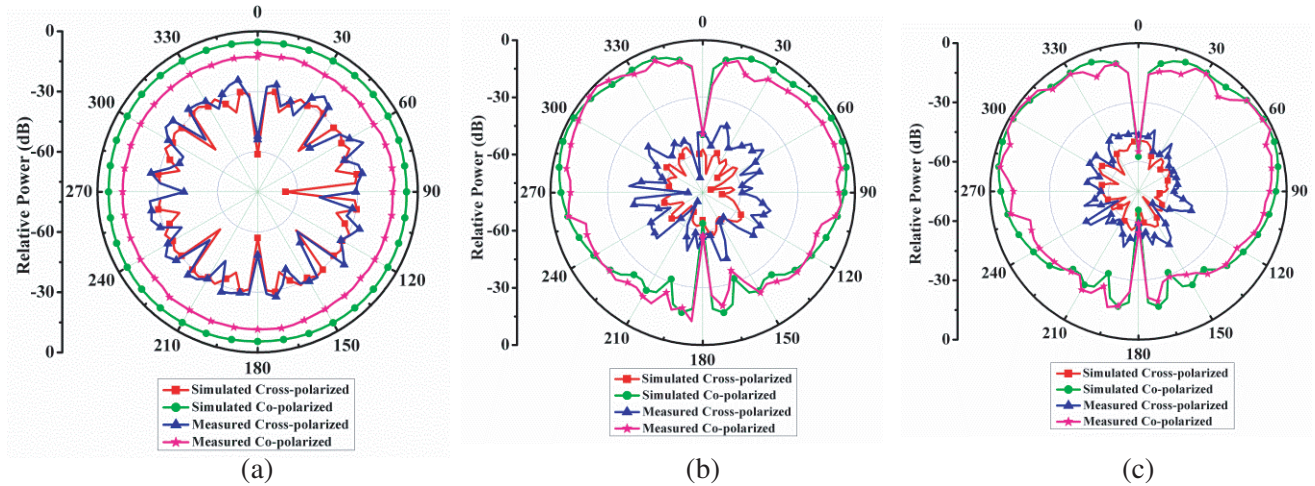


Figure 8. Radiation pattern of proposed two elements DS h-CDRA, (a) in ZX-plane, (b) in YZ-plane, (c) in XY-plane at frequency 8.0 GHz.

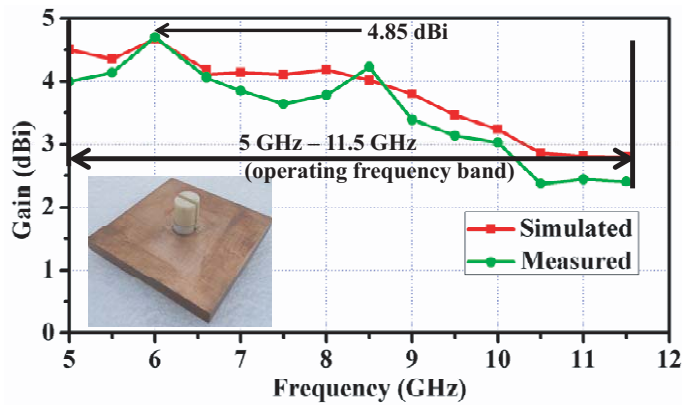


Figure 9. Variation of Gain vs. frequency curve of proposed two elements DS h-CDRA.

approximately a constant value throughout operating frequency band. The simulated radiation efficiency and peak directivity at the resonant frequency have been observed as 99% and 5.1 dB at resonant frequency respectively.

The RCS (Radar Cross Section) analysis of two-element dual-segment h-CDRA has been performed for both cases (Monostatic and Bistatic). In monostatic RCS versus theta for normal impinging plane (Iwave $\theta = 0^\circ$ and $\phi = 0^\circ$) as shown in Fig. 10, with the increase in theta, RCS decreases from 13 dB to -8 dB till 27° . After that the RCS increases to 2.5 dB at 45° , then again decreases to -0.5 dB at 55° and becomes constant to around 3.5 dB with increase in theta.

The bistatic RCS vs theta for normal impinging plane (Iwave $\theta = 0^\circ$ and $\phi = 0^\circ$) is shown in Fig. 11, and with increase in theta the RCS decreases from 13 dB to -8 dB at 60° . After that, the RCS increases up to 1 dB till 110° with a decrement in RCS up to 0 dB at 95° . RCS again increases after 125° and reaches up to 14 dB with increase in theta.

The bistatic RCS versus frequency curve is shown in Fig. 12. In Fig. 12 the monostatic RCS (Bistatic RCS at $\theta = 0^\circ$) versus frequency can be analyzed. From the curve it is clear that RCS is 7 dB at 4 GHz and increases up to 21 dB at 9.5 GHz. It can be seen that the RCS has been reduced twice, first at 10.3 GHz having RCS about 19.5 dB and the other decrement at 11.5 GHz having RCS about 19.5 dB again and that it increases rapidly with increase in frequency. On the other hand, for $\theta = 30^\circ$ to $\theta = 180^\circ$ except at $\theta = 60^\circ$, bistatic RCS increases with increase in frequency.

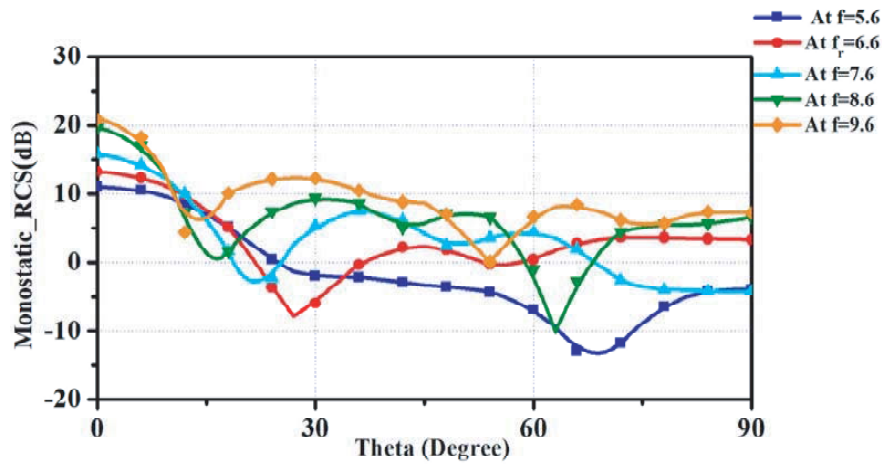


Figure 10. Monostatic normalized RCS versus theta curve of proposed two element dual segment h-CDRA at different frequencies.

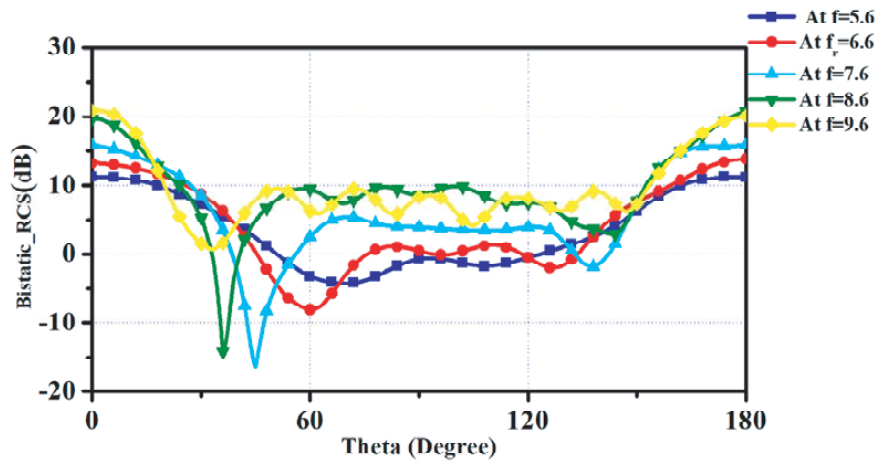


Figure 11. Bistatic normalized RCS versus theta curve of proposed two element dual segment h-CDRA at different frequencies.

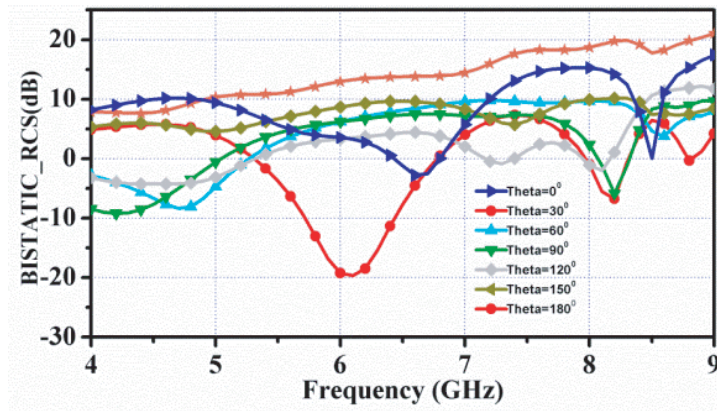


Figure 12. Bistatic normalized RCS versus frequency curve of proposed two element dual segment h-CDRA.

4. CONCLUSION

The paper concludes the design and fabrication of two elements DS h-CDRA and contrast of the input characteristics for DS h-CDRA. The proposed two elements DS h-CDRA gives wide bandwidth ($\sim 98\%$) and covers the entire 5.0 GHz WLAN and WiMAX band with uniform monopole type radiation pattern and achieves the gain of 4.85 dBi in operating band. The RCS analysis of the proposed antenna has been done for both monostatic and bistatic cases. The proposed antenna finds appropriate application in WLAN and WiMAX band.

ACKNOWLEDGMENT

Author Ravi Kumar Gangwar wishes to acknowledge Directorate of Extramural Research & Intellectual Property Rights (ER&IPR), DRDO, India for the financial support of this work through Extramural Research Grant project No. ERIP/ER/1303145/M/01/1549. Authors would like to acknowledge Prof. Dharmendra Singh, Department of Electronics and Communication Engineering, IIT Roorkee, India, for his guidance and also for providing his antenna measurement facility at IIT Roorkee.

REFERENCES

1. Petosa, A., *Dielectric Resonator Antenna Handbook*, Artech House, Boston, UK, 2007.
2. Long, A., A. Stuart, W. Mc. Mark, and L. C. Shen, "The resonant cylindrical dielectric cavity antenna," *IEEE Transactions on Antenna and Propagation*, Vol. 31, 406–412, 1983.
3. Kajfezand, D. and P. Guillon, *Dielectric Resonator*, Artech House, Norwood, MA, 1986.
4. Saedand, M. and R. Yadla, "Microstrip-fed low profile and compact dielectric resonator antennas," *Progress In Electromagnetics Research*, Vol. 56, 151–162, 2006.
5. Kishk, A. A., A. W. Glisson, and X. Zhang, "Analysis of a dielectric resonator antenna for wideband applications," *IEEE Transactions on Antennas and Propagation*, Vol. 50, 469–474, 2002.
6. Guha, D. and Y. M. M. Antar, "Four-element cylindrical dielectric resonator antenna for wideband monopole-like radiation," *IEEE Transaction on Antennas Propagation*, Vol. 54, 2657–2662, 2006.
7. Petosa, A., N. Simons, R. Siushansian, A. Ittipiboon, and M. Cuhaci, "Design and analysis of multisegment dielectric resonator antennas," *IEEE Transaction on Antennas Propagation*, Vol. 48, 738–742, 2000.
8. Luk, K. M. and S. M. Shum, "Stacked annular ring dielectric resonator antenna excited by axisymmetric coaxial probe," *IEEE Transactions on Antenna and Propagation*, Vol. 43, 889–892, 1995.
9. Guha, D., B. Gupta, C. Kumar, and Y. M. M. Antar, "Segmented hemispherical DRA: New geometry characterized and investigated in multi-element composite forms for wideband antenna applications," *IEEE Transactions on Antennas and Propagation*, Vol. 60, 1605–1610, 2012.
10. Gangwar, R. K., P. Ranjan, and A. Aigal, "Wideband four element two segment triangular dielectric resonator antenna with monopole-like radiation," *International Journal of Microwave and Wireless Technologies*, Vol. 9, No. 2, 411–418, 2017.
11. Mongia, R. K., "Half-split dielectric resonator placed on a metallic plane for antenna applications," *Electronics Letters*, Vol. 25, 462–464, 1989.
12. Mongia, R. K., A. Ittipiboon, and Y. M. M. Antar, "A Half-split cylindrical dielectric resonator antenna using slot-coupling," *IEEE Microwave and Guided Wave Letters*, Vol. 3, 38–39, 1993.
13. Kishk, A. A. and A. W. Glisson, "Bandwidth enhancement for split cylindrical dielectric resonator antennas," *Progress In Electromagnetics Research*, Vol. 33, 97–118, 2001.
14. Matthew, T. T. K. and D. R. Murch, "Compact circular sector and annular sector dielectric resonator antenna," *IEEE Transactions on Antennas and Propagation*, Vol. 47, 837–842, 1999.
15. Shum, S. M. and K. M. Luk, "Characteristics of dielectric ring resonator antenna with an air gap," *Electronics Letters*, Vol. 30, 277–278, 1994.

16. Junker, G. P., A. A. Kishk, A. W. Glisson, and D. Kajfez, "Effect of airgap on cylindrical dielectric resonator antenna operating in $TM_{01\delta}$ mode," *Electronics Letters*, Vol. 30, 97–98, 1994.
17. Kishk, A. A., A. W. Glisson, G. P. Junker, and D. Kajfez, "Effect of air-gap on cylindrical dielectric resonator antenna operating in $TM_{01\delta}$ mode," *Electronics Letters*, Vol. 30, 97–98, 1994.
18. Mongia, R. K., A. Ittipiboon, P. Bhartia, and M. Cuhaci, "Electric monopole antenna using a dielectric ring resonator," *Electronics Letters*, Vol. 29, 1530–1531, 1993.
19. Ittipiboon, A., A. Petosa, and S. Thirakoune, "Bandwidth enhancement of a monopole using dielectric antenna resonator loading," *Proc. ANTEM Conf.*, 387–390, Montreal, Canada, 2002.
20. Lapierre, M., Y. M. M. Antar, A. Ittipiboon, and A. Petosa, "Ultra wideband monopole/dielectric resonator antenna," *IEEE Microw. Wireless Comp. Lett.*, Vol. 15, 7–9, 2005.
21. Gangwar, R. K., S. P. Singh, and D. Kumar, "Four element wideband rectangular dielectric resonator antenna terminated in bio-medium," *Wireless Personal Communications: An International Journal*, Vol. 73, 663–677, 2013.
22. Gangwar, R. K., P. Ranjan, and A. Aigal, "Four element triangular dielectric resonator antenna for wireless application," *International Journal of Microwave and Wireless Technologies*, Vol. 9, No. 1, 133–119, 2017.
23. Balanis, C. A., *Antenna Theory and Design*, 3rd Edition, Wiley, New York, NY, USA, 2007.
24. Knott, E. F., J. F. Shaeffer, and M. T. Tuley, *Radar Cross Section*, 2nd Edition, SciTech Publishing, Inc., NC, 2004.
25. Joozdani, M. Z., M. K. Amirhosseini, and A. Abdolali, "Wideband radar cross-section reduction of patch array antenna with miniaturised hexagonal loop frequency selective surface," *Electron. Lett.*, Vol. 52, No. 9, 767–768, 2016.
26. Baskey, H. B., E. Johari, and M. J. Akhtar, "Metamaterial structure integrated with a dielectric absorber for wideband reduction of antennas radar cross section," *IEEE Trans. Electromagn. Compat.*, Vol. 59, No. 4, 1060–1069, 2017.
27. Zhao, Y., "In-band RCS reduction of waveguide slot array using metasurface bar," *IEEE Transactions on Antennas and Propagation*, Vol. 65, No. 2, 943–947, 2017.
28. Ranjan, P. and R. K. Gangwar, "Probe feed half split cylindrical dielectric resonator antenna for wideband application," *International Journal of Electronics and Communications-Elsevier*, Vol. 69, 1709–1714, 2015.